Ceramics International 42 (2016) 18087–18093

Contents lists available at ScienceDirect

Ceramics International

journal homepage: www.elsevier.com/locate/ceramint

Structural ordering and dielectric properties of $Ba_3CaNb_2O_9$-based microwave ceramics

J.E.F.S. Rodrigues [a,*], P.J. Castro [b], P.S. Pizani [c], W.R. Correr [a], A.C. Hernandes [a]

[a] Instituto de Física de São Carlos, Universidade de São Paulo, CEP 13560-970 São Carlos, SP, Brazil
[b] Laboratório Associado de Plasma, Instituto Nacional de Pesquisas Espaciais, CEP 12227-010 São José dos Campos, SP, Brazil
[c] Departamento de Física, Universidade Federal de São Carlos, CEP 13565-905 São Carlos, SP, Brazil

ARTICLE INFO

Article history:
Received 24 January 2016
Received in revised form
17 August 2016
Accepted 18 August 2016
Available online 20 August 2016

Keywords:
$Ba(Ca_{1/3}Nb_{2/3})O_3$
1:2 ordered perovskite
Cation ordering
Microwave dielectric properties
Dielectric resonator

ABSTRACT

$Ba_3CaNb_2O_9$ is a 1:2 ordered perovskite which presents a trigonal cell within the $D_{3d}{}^3$ space group. Dense ceramics of $Ba_3CaNb_2O_9$ were prepared by the solid-state reaction route, and their microwave dielectric features were evaluated as a function of the sintering time. From Raman spectroscopy, by using group-theory calculations, we were able to recognize the coexistence of the 1:1 and 1:2 ordering types in all samples, in which increasing the sintering time tends to reduce the 1:1 domain, leading to an enhancement of the unloaded quality factor. We concluded that this domain acts as a lattice vibration damping, consequently raising the dielectric loss at microwave frequencies. The best microwave dielectric parameters were determined in ceramics sintered at 1500 °C for 32h: $\varepsilon' \sim 43$; $Q_u \times f_r = 15{,}752$ GHz; $\tau_f \sim 278$ ppm °C^{-1}.

1. Introduction

Microwave dielectric ceramics are recognized materials with a wide application in wireless communication, including direct-broadcast TV, internet of things, global positioning system and military monitoring [1]. For higher performance, however, these materials should present high dielectric constant ε' for miniaturization, low dielectric loss to improve the selectivity at microwave regime and a near-zero value for the temperature coefficient of resonant frequency (τ_f in units of ppm °C^{-1}), enabling the thermal stability of the circuitry [2]. Also, the dielectric loss ($\tan\delta = Q_u{}^{-1}$, where Q_u is the quality factor) is strongly dependent on intrinsic (e.g. ionic polarization, crystalline structure) and extrinsic (e.g. vacancies, grain boundaries) features [3]. Notably, the complex perovskites, with chemical formula $A_3B'^{2+}B''^{5+}_2O_9$, are appropriate for microwave applications, since these ceramics fulfill the previous requirements. These systems may exhibit the structural ordering from a disordered cubic unit cell to one of a superstructure. When fully ordered, the cell adopts the trigonal structure within the $D_{3d}{}^3$ space group as a result of rhombohedral distortion along the $[111]_c$ cubic direction [4], with the lattice parameters $a_h = \sqrt{2}a_c$ and $c_h = \sqrt{3}a_c$ (a_c is the primitive cubic lattice parameter). When entirely disordered, the B'^{2+} and B''^{5+} ions are randomly distributed into the B-site of the cubic $Ba(B',B'')O_3$ perovskite. The occurrence of some degree of disorder in the D_{3d} trigonal unit cell is also possible, resulting in increased cell volume and crystal symmetry lowering [5].

Tantalum-based ceramics, like $Ba_3B'Ta_2O_9$ (B′=Mg, Zn), exhibits attractive Q_u values higher than 15,000 at 9–10 GHz [2,6]. However, the high cost of the tantalum oxide employed in the synthesis step increases the price of the final devices, so that the substitution of tantalum by niobium is an excellent alternative, since Nb^{5+} and Ta^{5+} ions have the similar ionic radii [7]. In the last decade, several authors have reported the ordering features in the physical-chemical properties of niobium-based perovskites. Particularly, the $Ba_3CaNb_2O_9$ system can exchange between microwave dielectric resonator and proton-conductor by tailoring the ordering degree of the crystal structure [8,9]. For proton-conducting, the mobility is correlated to the presence of the 1:1 ordered domain [10]. Although for many compositions, such as $Ba_3MgNb_2O_9$ [3] and $Ba_3ZnNb_2O_9$ [11], the microwave resonator properties have been widely reported, none of these features were investigated together with the structural ordering phenomena for the $Ba_3CaNb_2O_9$-based resonators. On top of that, the Raman spectroscopy technique has been used to probe the order/disorder effect and symmetry breakdown in ABO_3-based materials [12–14]. Therefore, our work investigates the effect of the variable structural ordering on the microwave performance of $Ba_3CaNb_2O_9$ dielectric resonator. We studied the ordering phenomena by combing the Raman spectroscopy and the group theoretical formalism seeking to elucidate possible correlations between structural ordering and dielectric resonator performance.

* Corresponding author.
E-mail address: rodrigues.joaoelias@gmail.com (J.E.F.S. Rodrigues).
URL: https://www.ifsc.usp.br (J.E.F.S. Rodrigues).

http://dx.doi.org/10.1016/j.ceramint.2016.08.113
0272-8842/

2. Experimental procedures

$Ba_3CaNb_2O_9$ (hereafter: BCaNO) powders were synthesized by conventional solid-state reaction following the principal steps. Stoichiometric quantities of $BaCO_3$ (Alfa Aesar; 99.80%), $CaCO_3$ (Alfa Aesar; 99.95%) and Nb_2O_5 (Alfa Aesar; 99.90%) were weighed and homogenized in a nylon jar containing isopropyl alcohol and zirconia cylinders for 24h. After a drying procedure at 100 °C, the mixture was calcined at 1300 °C for 2h in air atmosphere. The as-dried powders were mixed with a binder solution of polyvinyl butyral (3 wt%), pressed into cylinders (D = 12 mm × H = 5 mm) by uniaxial (15 MPa) and isostatic (300 MPa) cold pressing, and then sintered in air for different times (to obtain varying order ceramics) at 1500 °C, using heating and cooling rates of 5 °C min^{-1}. The resultant ceramics were polished to the dimensions of D ~ 11.2 mm × H ~ 3.6 mm. The phase identification of the ceramics was carried out by the X-ray powder diffraction (XRPD) technique (Cu-Kα = 1.54056 Å; 40 kV, 30 mA) using a Rigaku Rotaflex RU200B diffractometer over a 2θ range from 10° to 100° with a step size of 0.02° and a total exposure time of 2.5 h. The Raman scattering measurements were recorded by a *Jobin-Yvon* T64000 triple monochromator equipped with an LN_2 cooled charge coupled device (CCD) detector behind a 1800 grooves mm^{-1} grating (resolution ≤ 1 cm^{-1}). The signals were collected in a backscattering geometry using the 488 nm line of an argon laser (Coherent INNOVA 70C) as the excitation source and the power was kept below 2 mW and recorded after the 50 × objective. The micro-Raman spectra were divided by the Bose-Einstein thermal factor prior to the fitting procedure [15]. The Archimedes method was employed to obtain the bulk density of the ceramics. The microstructures were probed using an Inspect F50 field-emission scanning electron microscope (FEI, Netherlands) operating at 5 kV coupled to an energy dispersive X-ray spectrometer (EDS). The performance of the dielectric resonator was assessed using a cylindrical metallic cavity (gold coated) with an Agilent N5230C vector network analyzer. From this setup, both TE_{011} and $TE_{01\delta}$ modes were employed to obtain the dielectric constant (ε′) and the unloaded quality factor (Q_u) of the BCaNO ceramics [16]. This system was also placed in a temperature chamber (Weiss WKL/100) and the temperature coefficient of resonant frequency (τ_f) was obtained in an interval between 0 and 50 °C through the equation:

$$\tau_f = \frac{f_f - f_i}{f_i(T_f - T_i)}, \quad (1)$$

so that f_f and f_i denote the resonant frequencies at T_f (50 °C) and T_i (0 °C) temperatures, respectively. Additional information is available in the Supplementary Data.

3. Results and discussion

The XRPD patterns of the BCaNO ceramics sintered at 1500 °C for different times are depicted in Fig. 1. There is no evidence of secondary phase in all samples. The BCaNO ceramic sintered for 32h were indexed according to the 1:2 ordered perovskite structure belonging to the D_{3d}^3, (P-3*m*1 or #164), space group (ICSD #162758) with three chemical formulas per unit cell ($Z = 3$) [9,17]. In this structure, the Ca^{2+} and Nb^{5+} ions are alternately arranged in the form …/Ca/Nb/Nb/Ca/Nb/Nb/… along the $[001]_h$ hexagonal direction. As a consequence, the superlattice reflections are expected to appear in the XRPD diffraction pattern, being produced by planes whose *hkl* indices obey the rule $(2h + k + l) \neq 3n$ [18]. Indeed, low intensity peaks located at ~ 12.1° (001), 17.2° (100), 24.3° (002), 32.6° (111), 35.1° (200), 39.2° (112) and 41.1° (103) occurred in the diffraction pattern of the 32 h sintered ceramic, being ascribed to the earlier reflections [5,19]. Also, the lattice parameters were calculated as $a_h = 5.9014(7)$ Å and $c_h = 7.277(1)$ Å, leading to a theoretical density of 5.915 g cm^{-3}. Otherwise, none of the previous superlattice reflections was found in the diffraction pattern of the ceramic sintered for 2 h, indicating that the 1:2 ordered structure was not produced. In this case, two other crystal structures can be proposed to index the diffraction peaks: the first accounts for the fully disordered structure within the O_h^1, (P*m*-3*m* or #221), space group, in which the Ca^{2+} and Nb^{5+} ions are randomly distributed at the B-site, and the second corresponds to the 1:1 ordered structure within the O_h^5, (F*m*-3*m* or #225), space group (ICDD #49-0425), such that the cation ordering arises from the 1:1 order between Nb and (⅔Ca + ⅓Nb) [20]. For the 8 h

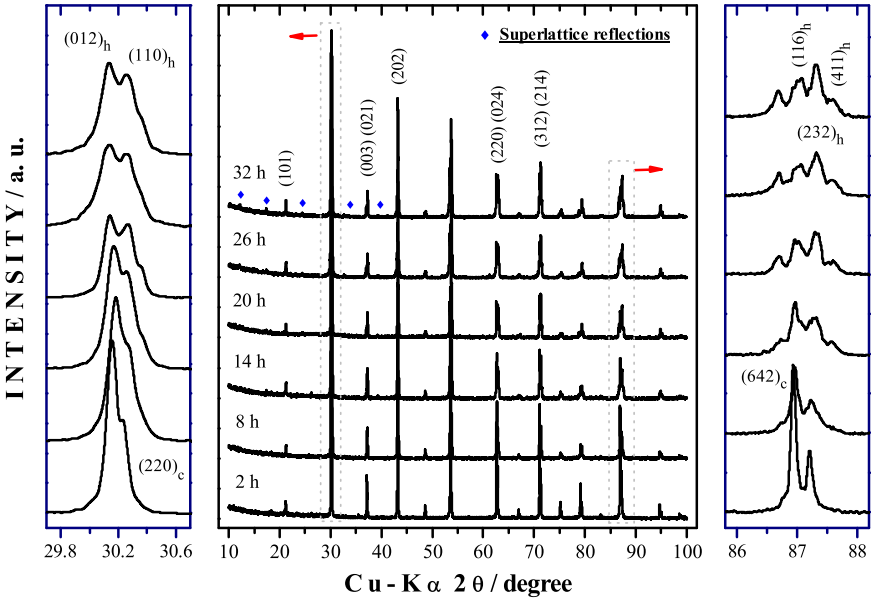

Fig. 1. XRPD patterns of the BCaNO ceramics sintered at 1500 °C for different times. The superlattice reflections (blue diamonds) were ascribed to the trigonal structure that belongs to the D_{3d}^3 space group. The main peak at ~ 30.2° splitted into two counterparts indexed as $(012)_h$ and $(110)_h$. (For interpretation of the references to color in this figure legend, the reader is referred to the web version of this article)

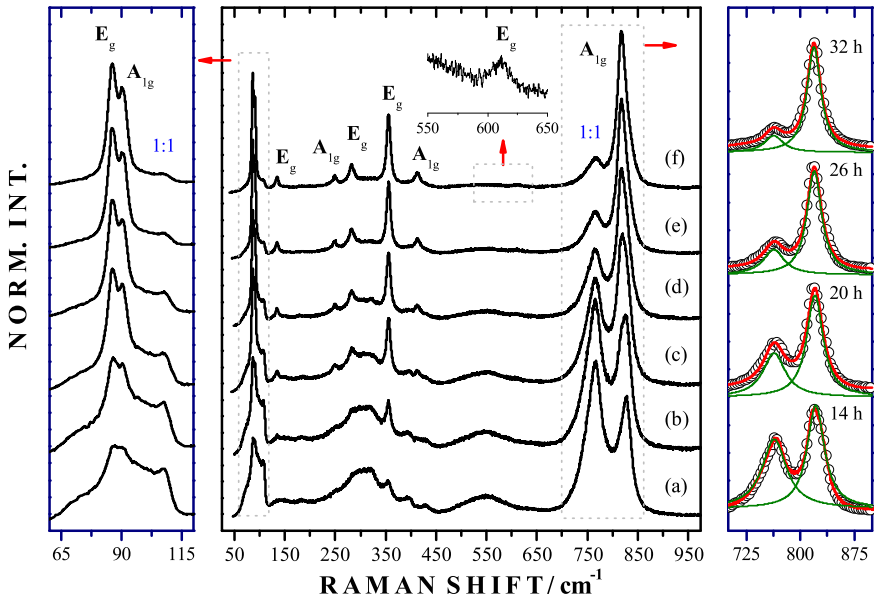

Fig. 2. Raman spectra at room temperature of the BCaNO ceramics sintered for 2 h (a), 8 h (b), 14 h (c), 20 h (d), 26 h (e) and 32 h (f). The black open circles represent experimental data and red and green lines denote the fitted spectrum using Lorentzian profiles. The inset shows the $\mathbf{E}_g(5)$ mode at 608 cm^{-1}. (For interpretation of the references to color in this figure legend, the reader is referred to the web version of this article)

sintered ceramic, the last crystal structure is more appropriate to index its diffraction pattern, since a high degree of ordering is expected after long-time sintering [21,22]. It is important to highlight that the splitting of some diffraction peaks occurred at ~ 30.2° and ~ 87.1° (2θ), as depicted in details of Fig. 1. The main peak labeled as $(220)_c$ splitted into two counterparts indexed as $(012)_h$ and $(110)_h$ and derived from the trigonal unit cell in the BCaNO sintered ceramics for, at least, 14 h [4]. This phenomenon was attributed to a gradual change in the ordering at B-site from 1:1 (cubic) to 1:2 (trigonal) type, determining the role of the sintering time in the ordering behavior. To probe this process, the Raman spectroscopy measurements were recorded in all samples to better understand the correlation between the ordered structure and the lattice vibration modes of the BCaNO ceramics.

The Raman spectra at room temperature of the as-sintered BCaNO ceramics are shown in Fig. 2. There is a continuous change in the spectra when the sintering time is increased until 32 h, especially two bands centered at 763 and 819 cm^{-1}. Three low wavenumber bands at 65–115 cm^{-1} also depicted some modifications, for example the intensity of the band at 105 cm^{-1} is reduced when the sintering time is increased. The Raman bands belonging to the wavenumber range 200–450 cm^{-1} also featured a continuous definition as a function of the sintering time. For further analysis of the ordering, the group-theoretical tools were taken into account to predict the Raman and infrared (IR) modes at the Γ point in terms of the irreducible representation of the D_{3d} and O_h factor groups [23]. As illustrated in Table 1, 9 Raman-active modes ($4\mathbf{A}_{1g} \oplus 5\mathbf{E}_g$) and 16 IR-active modes ($7\mathbf{A}_{2u} \oplus 9\mathbf{E}_u$) are expected for the BCaNO lattice with 1:2 ordered cell. Instead, 4 Raman-active modes ($\mathbf{A}_{1g} \oplus \mathbf{E}_g \oplus 2\mathbf{F}_{2g}$) and 4 IR-active modes ($4\mathbf{T}_{1u}$) are predicted to appear in the vibrational spectra of the BCaNO ceramic with 1:1 ordered cubic structure. It is important to point out that the Raman modes are only due to the motions of Ba^{2+} and Nb^{5+} cations at the 2*d* sites and O^{2-} anions at the 6*i* sites within the D_{3d} trigonal structure. In the case of the cubic cell, the Raman-active bands arise from the motions of Ba^{2+} cations at 8*c* sites and O^{2-} anions at the 24*e* sites. Therefore, the ordering behavior can be evaluated by monitoring the Raman bands of the BCaNO ceramics, since the sintering process for several times gradually turns the type of ordering and then the number of the bands.

Table 1
Factor group analysis for the $Ba_3CaNb_2O_9$ system in agreement with the ordered structures discussed in this work.

Ion	Wyckoff position	Site symmetry	Irreducible representation
Cubic: *Fm*-3*m*, O_h^5 or #225			
Ba^{2+}	8*c*	T_d	$\mathbf{F}_{1u} \oplus \mathbf{F}_{2g}$
Ca^{2+} / Nb^{5+}	4*a*	O_h	$\mathbf{F}_{1u}$
Nb^{5+}	4*b*	O_h	$\mathbf{F}_{1u}$
O^{2-}	24*e*	C_{4v}	$\mathbf{A}_{1g} \oplus \mathbf{E}_g \oplus \mathbf{F}_{1g} \oplus 2\mathbf{F}_{1u} \oplus \mathbf{F}_{2g} \oplus \mathbf{F}_{2u}$
$\Gamma_{TOTAL} = \mathbf{A}_{1g} \oplus \mathbf{E}_g \oplus \mathbf{F}_{1g} \oplus 2\mathbf{F}_{2g} \oplus 5\mathbf{F}_{1u} \oplus \mathbf{F}_{2u}$			$\Gamma_{ACOUSTIC} = \mathbf{F}_{1u}$
$\Gamma_{RAMAN} = \mathbf{A}_{1g} \oplus \mathbf{E}_g \oplus 2\mathbf{F}_{2g}$			$\Gamma_{IR} = 4\mathbf{F}_{1u}$
Trigonal: P-3*m*1, D_{3d}^3 or #164			
Ba^{2+}	1*b*	D_{3d}	$\mathbf{A}_{2u} \oplus \mathbf{E}_u$
Ba^{2+}	2*d*	C_{3v}	$\mathbf{A}_{1g} \oplus \mathbf{A}_{2u} \oplus \mathbf{E}_g \oplus \mathbf{E}_u$
Ca^{2+}	1*a*	D_{3d}	$\mathbf{A}_{2u} \oplus \mathbf{E}_u$
Nb^{5+}	2*d*	C_{3v}	$\mathbf{A}_{1g} \oplus \mathbf{A}_{2u} \oplus \mathbf{E}_g \oplus \mathbf{E}_u$
O^{2-}	3*f*	C_{2h}	$\mathbf{A}_{1u} \oplus 2\mathbf{A}_{2u} \oplus 3\mathbf{E}_u$
O^{2-}	6*i*	C_S	$2\mathbf{A}_{1g} \oplus \mathbf{A}_{1u} \oplus \mathbf{A}_{2g} \oplus 2\mathbf{A}_{2u} \oplus 3\mathbf{E}_g \oplus 3\mathbf{E}_u$
$\Gamma_{TOTAL} = 4\mathbf{A}_{1g} \oplus \mathbf{A}_{2g} \oplus 5\mathbf{E}_g \oplus 2\mathbf{A}_{1u} \oplus 8\mathbf{A}_{2u} \oplus 10\mathbf{E}_u$			$\Gamma_{ACOUSTIC} = \mathbf{A}_{2u} \oplus \mathbf{E}_u$
$\Gamma_{RAMAN} = 4\mathbf{A}_{1g} \oplus 5\mathbf{E}_g$			$\Gamma_{IR} = 7\mathbf{A}_{2u} \oplus 9\mathbf{E}_u$

Visually, the Raman spectrum of the BCaNO ceramic sintered for 2 h exhibits a set of 5 broad bands at 90, 300, 550, 750 and 820 cm^{-1}, whereas a total of 11 bands were noted in the spectrum of the ceramic sintered during 32 h, as listed in Table 2. In addition, the Raman spectra of the remaining ceramics presented defined bands as the sintering time increased. These experimental observations corroborate the recent literature, see Refs. [13,22], and point out the structural order transition from 1:1 (cubic) to 1:2 (trigonal) order depending on the sintering time. From Table 1, 9 of 11 Raman bands of the BCaNO ceramic sintered for 32 h are in accordance with previous calculations using the density functional perturbation theory [22]. These modes are concerned with the external vibrations of Ba^{2+} ions against O^{2-} anions, appearing at 86 and 91 cm^{-1} in the Raman spectra. Also, the bands centered at 413 and 820 cm^{-1} are called the internal modes denoting the

Table 2
Experimental Raman bands at room temperature for the BCaNO ceramic sintered at 1500 °C for 32 h, in which $\tilde{\nu}$ and γ denote the position and width of the phonon mode, respectively. We have also compared the experimental (expt.) and calculated (calc.) data [22].

Band No.	$\tilde{\nu}$ (expt.) (cm^{-1})	γ (expt.) (cm^{-1})	$\tilde{\nu}$ (calc.) (cm^{-1})	Symmetry
1	86	2.2 ± 0.1	59	$\mathbf{E}_g(1)$
2	91	2.0 ± 0.1	60	$\mathbf{A}_{1g}(1)$
3	105	5.4 ± 0.6	–	1:1 domain
4	134	2.4 ± 0.3	62	$\mathbf{E}_g(2)$
5	249	4.8 ± 0.4	241	$\mathbf{A}_{1g}(2)$
6	282	7.1 ± 0.2	251	$\mathbf{E}_g(3)$
7	356	5.0 ± 0.1	306	$\mathbf{E}_g(4)$
8	412	6.1 ± 0.4	357	$\mathbf{A}_{1g}(3)$
9	608	9.0 ± 3.0	659	$\mathbf{E}_g(5)$
10	763	15.5 ± 0.1	–	1:1 domain
11	819	11.7 ± 0.1	828	$\mathbf{A}_{1g}(4)$

stretching and breathing vibrations of the NbO_6 octahedra, respectively, whereas the internal mode appearing at 356 cm^{-1} is related to the twisting breath-vibrations of oxygen octahedron. The remaining Raman bands centered at 134, 249, 282 and 608 cm^{-1} depict the modes attributed to the trigonal structure, indicating the formation of the 1:2 ordering at long-range in the BCaNO ceramic sintered for 32 h. While the number of the experimental modes is higher than for the predicted, the Raman bands at 105 and 763 cm^{-1} can be designated as disorder induced modes, as will be discussed later.

It is well known that the disorder at the A- and/or B-sites in the perovskites usually promotes a local breakdown of the crystal symmetry and, as a consequence, the Raman spectrum tends to exhibit an higher number of experimental bands [13,24]. This phenomenon is explained in light of the loss of some symmetry operations, resulting in a structural transition from a high to low symmetry phase [14,25]. In the case of the 1:2 trigonal structure, the partial disorder can occur when Ca^{2+} and Nb^{5+} ions exchange their Wyckoff positions, leading to an increase in the phonon distribution at the Γ point. Particularly, two new Raman and four new IR bands should occur in the vibrational spectra of the BCaNO ceramics with partial disorder, once Ca^{2+} ions at 2*d* sites provide $\Gamma_{Ca/2d} = \mathbf{A}_{1g} \oplus \mathbf{E}_g \oplus \mathbf{A}_{2u} \oplus \mathbf{E}_u$ and Nb^{5+} ion at 1*b* site gives $\Gamma_{Nb/1b} = \mathbf{A}_{2u} \oplus \mathbf{E}_u$ [17]. The previous model was successfully applied by Moreira et al. to account for the Raman spectra of the $Ba_3MgNb_2O_9$ ceramics from powders obtained by hydrothermal synthesis [12]. In contrast, the Raman modes induced by the partial disorder can also be ascribed to the coexistence of 1:1 and 1:2 ordering types in the crystal structure. According to Blasse el al. [26], the occurrence of the bands at 790 and 830 cm^{-1} in the Raman spectrum of the $Sr_3CaNb_2O_9$ perovskite can be justified by considering two Nb octahedra with different surroundings (domains), depending on the ordering type. Notably, the band at 790 cm^{-1} was attributed to the 1:1 ordered domains, while the band at 830 cm^{-1} was related to the 1:2 ordered ones.

As presented in Table 1, the B-site ions in the 1:1 (cubic) ordered perovskite are located at O_h (4*a* and 4*b*) sites and, then, the niobium octahedra possess symmetric surroundings. Instead, the Nb^{5+} ions within the trigonal cell are located at C_{3v} sites and, then, with asymmetric surroundings. Both the niobium octahedron types (domains) can be found in the 1:2 trigonal structure with some degree of disorder [26]. Since the Raman spectra depicted in Fig. 2 more closely resemble those reported by Blasse for the $Sr_3CaNb_2O_9$ perovskite, we concluded that the BCaNO sintered ceramics exhibited a reduction of the 1:1 ordered domain as the sintering time was increased up to 32 h. A piece of evidence for this behavior came from the splitting of the $(220)_c$ diffraction peak at the same time that the intensity of the Raman band at 819 cm^{-1} becomes higher than the band intensity at 763 cm^{-1}. Similar results were reported by Du et al. concerning the $A_3Ca_{1+x}Nb_{2-x}O_{9-\delta}$ perovskites (A = Ba, Sr), in which the non-stoichiometry promoted a structural order transition from 1:2 to 1:1 order, enhancing the proton conduction and making them promising candidates for solid oxide fuel cell applications [10,27,28]. In our study, however, the sintering time drives the coexistence of 1:1 and 1:2 ordering types. In order to probe the 1:1 ordered domain effects on the dielectric properties of the BCaNO perovskite, we performed the microwave resonator measurements of the BCaNO ceramics and the results were further associated with the bulk density (ρ) and grain size distribution (D_g), as discussed below.

The bulk densities of the BCaNO ceramics sintered at 1500°C during 2 up to 32 h are summarized in Table S2 of Supplementary Data. The theoretical density estimated from the XRPD pattern was applied to calculate the relative density (ρ). As one can see, the obtaining of dense ceramics (> 90%) was only possible after 20 h of sintering. Such result means that the sintering time not only reduces the 1:1 ordered domains, but also raises the relative density. Fig. 3(a) depicts the sintering temperature dependence of the porosity (= 1 − ρ) obtained from Archimedes' principle. It can be pointed out that the porosity decreases until 9% after 20 h, suggesting the formation of closed pores in BCaNO samples. Indeed, a near-zero open porosity was found in samples sintered at dwell times greater than 20 h. The microstructures of the BCaNO ceramics were evaluated by means of the scanning electron microscopy and some representative micrographs are illustrated in Fig. 4(a–f). The polished and thermally etched surfaces exhibited a honeycomb-like structure without clear grain boundary grooves, excluding the samples sintered at dwell times less than 20 h. It should be observed that some grains exhibit an anisotropic grain growth, as can be seen in G1, G2 and G3. Also, there are no signals of the liquid phase formation and/or impurity at the grain

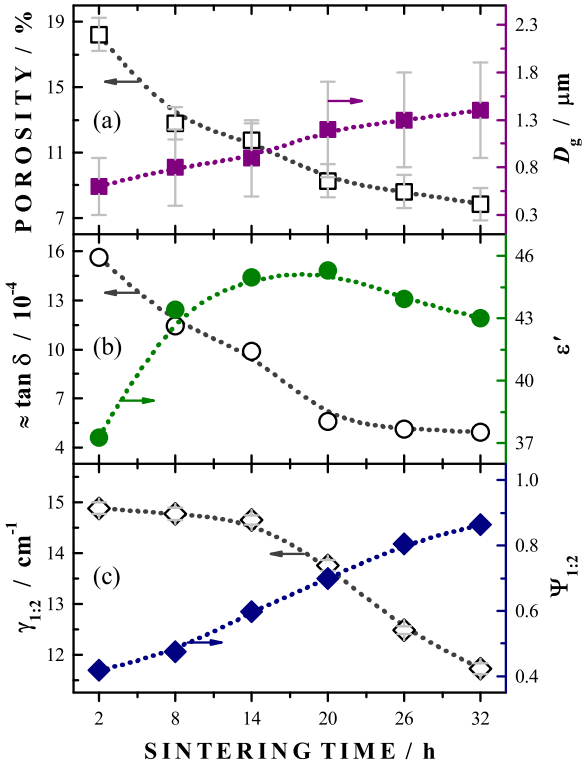

Fig. 3. Dependence of (a) the porosity and average grain size (D_g); (b) dielectric loss and relative permittivity (ε′); (c) $\mathbf{A}_{1g}(4)$ width ($\gamma_{1:2}$) and ratio $\Psi_{1:2}$ with the sintering time.

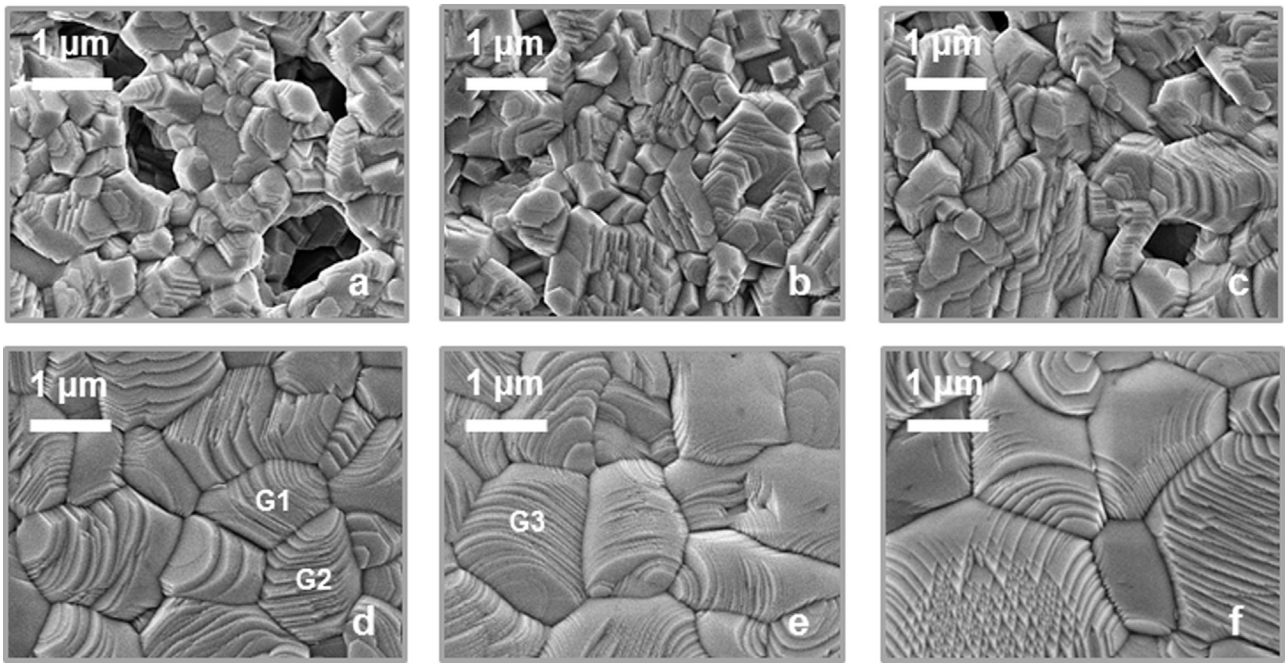

Fig. 4. Scanning electron micrographs of the BCaNO ceramics after thermal etching and varying sintering time: 2 h (a), 8 h (b), 14 h (c), 20 h (d), 26 h (e) and 32 h (f) (scale bars 1μm). All micrographs were generated by the back-scattered electron (BSE) mode.

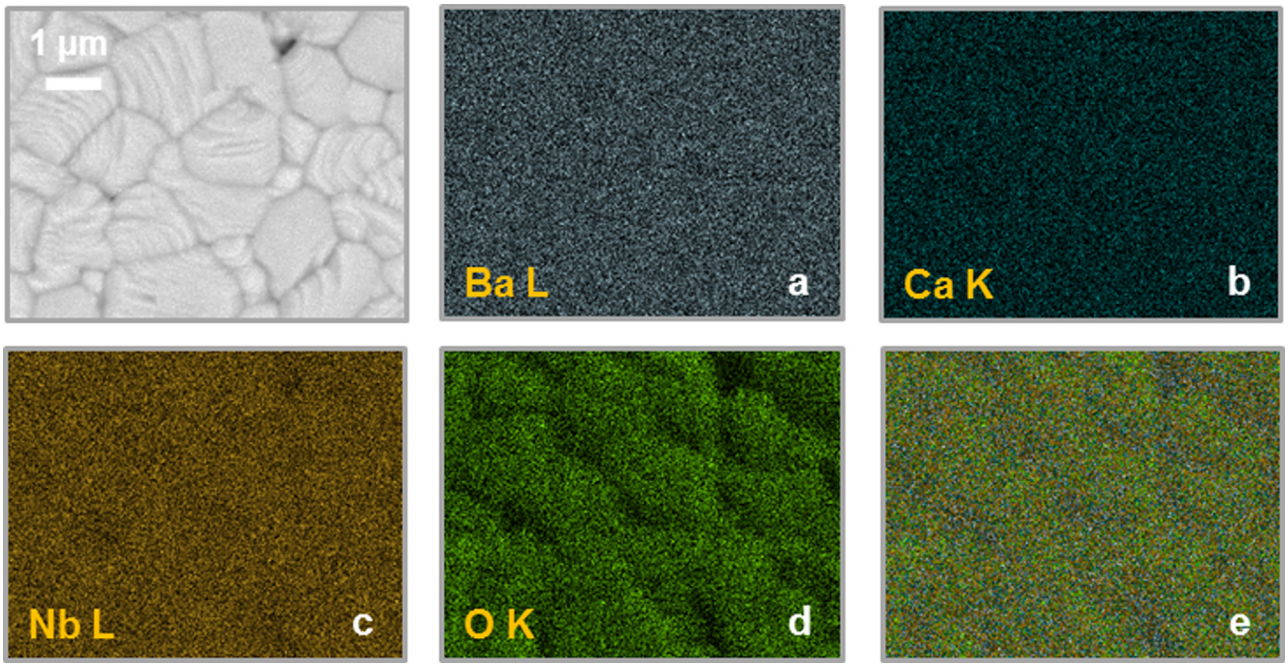

Fig. 5. EDS elemental mapping for Ba (a), Ca (b), Nb (c) O (d), and their color superposition (e) toward the SEM micrograph on the left of the 32 h BCaNO ceramic (scale bars 1μm).

boundaries, as confirmed by the EDS analysis, in which the elemental mapping of the Ba (L), Ca (K), and Nb (L) and O (K) elements revealed a homogenous distribution of those atoms in the microstructures (see Fig. 5(a–e)). Not surprisingly, the grain size distribution was well fitted by the log-normal distribution, from which the average grain size (AGS or D_g) and the standard deviation (w_g) of the log-normal function were extracted, as listed in Table 3. Fig. 3(a) displays the sintering time dependence of the average grain size. The data exhibits an almost linear behavior with dwell time, denoting that it is possible to tune the AGS parameter just by changing the sintering time. Furthermore, the AGS was elevated from 0.6μm (2 h) to 1.4μm (32 h). We concluded that the sintering process induced a normal grain growth, since the w_g value remains almost constant [29].

The dielectric microwave properties of the BCaNO ceramics are summarized in Table 3. Fig. 3(b) displays the sintering time dependence of the relative permittivity (ε′) acquired from the cylindrical cavity method. The permittivity reached a value around 44 ± 1, which means that the BCaNO ceramics present higher ε′ values than those reported for some members of the 1:2 ordered perovskite family, such as $Ba_3MgNb_2O_9$ (ε′ ~ 31) and $Ba_3ZnNb_2O_9$ (ε′ ~ 41) [30,31]. Also, there is a clear increase in the quality factor

Table 3
List of microstructural parameters (relative density and average grain size) and microwave dielectric properties the BCaNO ceramics.

Ceramic	Microstructural data		Microwave properties			
Sintering time	ρ (%)	D_g (μm) / w_g	ε′	$Q_u \times f_r$ (GHz)	f_r (GHz)	τ_f (ppm °C^{-1})
2 h	82 ± 1	0.6 / 0.3	37	4,987	7.81	–
8 h	87 ± 1	0.8 / 0.4	43	6,246	7.15	–
14 h	88 ± 1	0.9 / 0.4	45	7,497	7.40	250
20 h	91 ± 1	1.2 / 0.5	45	13,978	7.80	276
26 h	91 ± 1	1.3 / 0.5	44	14,783	7.60	277
32 h	92 ± 1	1.4 / 0.5	43	15,752	7.76	278

(Q_u) from 4,987 GHz [at 7.81 GHz] for ceramics fired at 1500 °C for 2 h to 15,752 GHz [at 7.76 GHz] for ceramics sintered at 1500 °C for 32 h. Since the relative densities of the BCaNO samples fired for 20 up to 32 h have similar values (~ 91%), it can be postulated that the 1:2 domain contributes to the Q_u improvement. In accordance with the classical dispersion theory, the dielectric loss at microwave region can be estimated using the next relation:

$$\tan\delta \propto \left(\sum_i \frac{\xi_i \lambda_i}{\omega_i^2}\right)\omega, \tag{2}$$

so that ξ_i, λ_i and ω_i denote the dispersion parameters: strength, damping factor and the resonance frequency of each oscillator [32]. The earlier expression corroborates the fact that anharmonicity of the lattice is the main reason for the loss [3,33]. Fig. 3 (b) depicts the sintering time dependence of the dielectric loss at microwave frequencies. It is clear that the loss monotonically decreases to a value of ~ 5×10^{-4} for 32 h sintered ceramic. Theoretically, the damping factor acts by reducing the phonon-lifetime (ζ). From the energy uncertainty relationship [34,35], one can see that the bandwidth (γ) is inversely related to the phonon-lifetime, and thus directly related to the lattice damping. Although the microwave features of a dielectric resonator are mostly affected by extrinsic factors such as secondary phase, porosity and grain size distribution [36], obtaining the low loss perovskite based-resonators also depends on the structural features [3,37]. Being such, we concluded that the increase of the sintering time softens the anharmonicity of the lattice, decreasing the dielectric loss and raising the phonon-lifetime.

Evidence for this behavior comes from the fact that the $\mathbf{A}_{1g}$ mode at 819 cm^{-1} became narrower as sintering time increased (see Fig. 3(c)). As mentioned previously, the reduction of the 1:1 ordered domain also depends on the dwell time. This trend can be exploited by using the ratio of peak intensities designated by $\Psi_{1:2}$ and defined as follows:

$$\Psi_{1:2} = \frac{I_{819}}{I_{763} + I_{819}}. \tag{3}$$

If the ratio $\Psi_{1:2}$ is equal to one, then only 1:2 domain must occur in the BCaNO ceramics. Therefore, the coexistence of 1:1 and 1:2 ordered domains leads to a ratio $\Psi_{1:2}$ less than one [17,22]. Fig. 3 (c) exhibits the correlation between ratio $\Psi_{1:2}$, obtained from Eq. (3), and dwell time. The behavior of this ratio depicted a linear increase with sintering time, confirming that the niobium octahedra gradually turn their surroundings ($O_h \rightarrow C_{3v}$). Therefore, we concluded that the microwave performance of the BCaNO ceramics is clearly affected by intrinsic factors, such as lattice vibration and 1:1 domain, and extrinsic factors, such as porosity, grain size, and so on. The 1:1 domain may introduce damping effects in the lattice vibrations, thus increasing the dielectric loss. Physically, it means that the 1:1 ordered domain acts as friction, inducing an increase in power loss at the resonance. In this way, the microwave

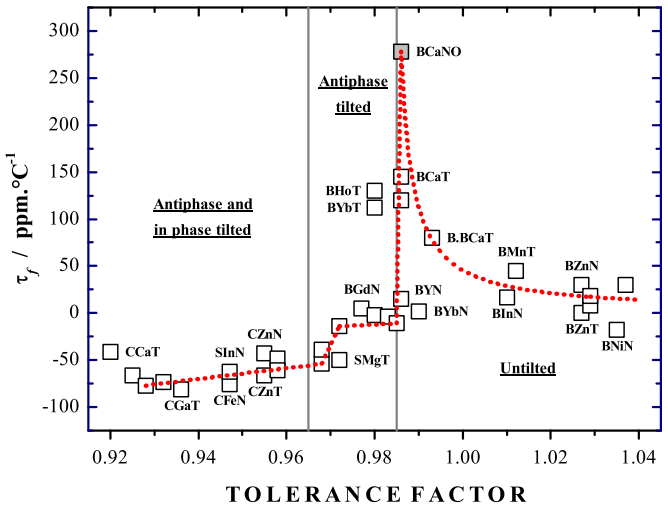

Fig. 6. Temperature coefficient of resonant frequency (τ_f) versus tolerance factor (t) for A(B′,B″)O_3 (A = Ca, Sr, Ba; B′ = Mg, Ca, Mn, Fe, Ni, Zn, Ga, In, Y, Gd, Tb, Dy, Ho, Er, Yb; B″ = Nb, Ta) 1:1 and 1:2 complex perovskites. The τ_f values are those summarized in Ref [1]. The dashed red line is a guide for the eye.

propagation in the BCaNO ceramics strongly depends on the properties of the oxygen octahedral network, particularly the phonon-lifetime and the local surrounding (ratio $\Psi_{1:2}$).

Finally, the temperature coefficient of resonant frequency (τ_f) was determined in the temperature range between 0 and 50 °C (see Table 3). The τ_f achieved a value about 277 ppm °C^{-1}, except for the BCaNO sintered for 14 h (τ_f~250 ppm °C^{-1}). It is noteworthy that τ_f parameter depends on the structural phase transitions driven by octahedral tilting [38]. Such transitions occur when BO_6 octahedra rotate either in phase or antiphase while maintaining their corner-sharing connectivity [39]. In particular, the temperature of the onset of octahedral tilt transitions depends on the tolerance factor (t) [40]. Fig. 6 shows a graph of τ_f values versus tolerance factor for several ordered perovskites, including the BCaNO system ($t \approx 0.986$). It can be noted that the BCaNO perovskite follows the general trend of the curve in the range $0.985 < t < 1.04$. According to Reaney et al. [40], the steep decrease in τ_f at $t \approx 0.985$ is concerned with the onset of an antiphase tilting of the oxygen octahedra. Since the BCaNO is located at this onset, a high value of τ_f is expected. It may, in future studies, be possible to discern the role of tilting transition in the BCaNO by high-resolution transmission electron microscopy. Furthermore, this highly positive τ_f should be appropriated to manufacture microwave components based on composites with negative τ_f values, like $Ba_3CoNb_2O_9$ (−10 ppm °C^{-1}) or $Sr_3ZnNb_2O_9$ (−35 ppm °C^{-1}) [41,42]. Similar approach was recently applied by Zhang et al. [43] to develop the stacking layered composite ceramics with $\tau_f \sim 0$ ppm °C^{-1}.

4. Conclusions

The XRPD and Raman spectroscopy studies of $Ba_3CaNb_2O_9$ ceramics sintered at 1500 °C under different times exhibited a coexistence of the ordering at B-site of 1:1 (cubic) and 1:2 (trigonal) domains. However, a partial migration in the ordered domains from 1:1 to 1:2 induced by the sintering time was also observed. The best microwave dielectric characteristics were obtained in the BCaNO ceramic sintered at 1500 °C for 32 h with ε′ ~ 43; $Q_u \times f_r$ = 15,752 GHz; $\tau_f \sim 278$ ppm °C^{-1}. Indeed, the high $|\tau_f|$ value is a negative feature of the BCaNO system. It is possible to predict that such disadvantage can be solved by using stacking layered composite to obtain ceramic bodies with almost zero

temperature coefficient of resonant frequency. We concluded that the 1:1 domain introduces a power loss at the resonance, which comes from the damping effect of the crystal lattice. Furthermore, we can conclude that there is a strong correlation between structural ordering and microwave dielectric properties.

Acknowledgments

The authors are grateful to the Brazilian funding agencies: CAPES, INCTMN (Proc. Number 2008/57872-1), CNPq (Proc. Number 573636/2008-7) and FAPESP (Proc. Number 2013/07296-2). J.E. Rodrigues acknowledges E.C. Domenicucci for the technical support.

Appendix A. Supplementary material

Supplementary data associated with this article can be found in the online version at http://dx.doi.org/10.1016/j.ceramint.2016.08.113.

References

[1] M. Sebastian, Dielectric Materials for Wireless Communication, 1st ed., Elsevier, United States, 2008.
[2] I.M. Reaney, D. Iddles, Microwave dielectric ceramics for resonators and filters in mobile phone networks, J. Am. Ceram. Soc. 89 (2006) 2063–2072.
[3] A. Dias, R.L. Moreira, Far-infrared spectroscopy in ordered and disordered $BaMg_{1/3}Nb_{2/3}O_3$ microwave ceramics, J. Appl. Phys. 94 (2003) 3414.
[4] J. Galasso, F. Pyle, Ordering in compounds of the $A(B'_{0.33}Ta_{0.67})O_3$ type, Inorg. Chem. 2 (1963) 482–484.
[5] C.-H. Wang, X.-P. Jing, L. Wang, J. Lu, XRD and Raman studies on the ordering/disordering of $Ba(Mg_{1/3}Ta_{2/3})O_3$, J. Am. Ceram. Soc. 92 (2009) 1547–1551.
[6] F. Azough, R. Freer, D. Iddles, T. Shimada, B. Schaffer, The effect of cation ordering and domain boundaries on low loss $Ba(B^{I}_{1/3}B^{II}_{2/3})O_3$ perovskite dielectrics revealed by high-angle annular dark-field scanning transmission electron microscopy (HAADF STEM), J. Eur. Ceram. Soc. 34 (2014) 2285–2297.
[7] R.C. Pullar, The synthesis, properties, and applications of columbite niobates ($M^{2+}Nb_2O_6$): a critical review, J. Am. Ceram. Soc. 92 (2009) 563–577.
[8] O. Valdez-Ramírez, F. Gómez-García, M.A. Camacho-López, E. Ruiz-Trejo, Influence of the calcium excess in the structural and spectroscopic properties of the complex perovskite $Ba_3CaNb_2O_9$, J. Electroceram. 28 (2012) 226–232.
[9] J. Deng, J. Chen, R. Yu, G. Liu, X. Xing, S. Han, et al., Neutron powder diffraction study and B-site ordering in microwave dielectric ceramics $Ba(Ca_{1/3}Nb_{2/3})O_3$, Solid State Sci. 11 (2009) 170–175.
[10] Y. Du, A.S. Nowick, Structural transitions and proton conduction in non-stoichiometric $A_3B'B''O_9$ perovskite-type oxides, J. Am. Ceram. Soc. 78 (1995) 3033–3039.
[11] C.-T. Lee, Y.-C. Lin, C.-Y. Huang, C.-Y. Su, C.-L. Hu, Cation ordering and dielectric characteristics in barium zinc niobate, J. Am. Ceram. Soc. 90 (2007) 483–489.
[12] R.L. Moreira, F.M. Matinaga, A. Dias, Raman-spectroscopic evaluation of the long-range order in $Ba(B'_{1/3}B''_{2/3})O_3$ ceramics, Appl. Phys. Lett. 78 (2001) 428.
[13] A. Dias, R.G. Sá, R.L. Moreira, Disorder-induced symmetry lowering in $Ba(Y_{1/2}Nb_{1/2})O_3$ ceramics probed by Raman spectroscopy, J. Raman Spectrosc. 39 (2008) 1805–1810.
[14] M. Abrashev, A. Litvinchuk, M. Iliev, R. Meng, V. Popov, V. Ivanov, et al., Comparative study of optical phonons in the rhombohedrally distorted perovskites $LaAlO_3$ and $LaMnO_3$, Phys. Rev. B 59 (1999) 4146–4153.
[15] W. Hayes, R. Loudon, Scattering of Light by Crystals, Dover, New York, 2004.
[16] D. Kajfez, P. Guillon, Dielectric Resonators, 2nd ed, SciTech Publishing, United States, 1998.
[17] J.E.F.S. Rodrigues, D. Morais Bezerra, A. Pereira Maciel, C.W.A. Paschoal, Synthesis and structural ordering of nano-sized $Ba_3B'Nb_2O_9$ (B′ = Ca and Zn) powders, Ceram. Int. 40 (2014) 5921–5930.
[18] S. Janaswamy, G. Sreenivasa Murthy, E. Dias, V.R. Murthy, Structural analysis of $BaMg_{1/3}(Ta,Nb)_{2/3}O_3$ ceramics, Mater. Lett. 55 (2002) 414–419.
[19] J. Deng, J. Chen, R. Yu, G. Liu, X. Xing, Crystallographic and Raman spectroscopic studies of microwave dielectric ceramics $Ba(Ca_{1/3}Nb_{2/3})O_3$, J. Alloy. Compd. 472 (2009) 502–506.
[20] G. Blasse, New compounds with perovskite-like structures, J. Inorg. Nucl. Chem. 27 (1965) 993–1003.
[21] C. Lu, C. Tsai, Reaction kinetics, sintering characteristics, and ordering behavior of microwave dielectrics: Barium magnesium tantalate, J. Mater. Res. 11 (1996) 1219–1227.
[22] J.E.F.S. Rodrigues, E. Moreira, D.M. Bezerra, A.P. Maciel, C.W. de Araujo Paschoal, Ordering and phonons in $Ba_3CaNb_2O_9$ complex perovskite, Mater. Res. Bull. 48 (2013) 3298–3303.
[23] D.L. Rousseau, R.P. Bauman, S.P.S. Porto, Normal mode determination in crystals, J. Raman Spectrosc. 10 (1981) 253–290.
[24] S.P. Marcondes, J.E.F.S. Rodrigues, M.R.B. Andreeta, A.C. Hernandes, Resonance Raman spectroscopy of $NdAlO_3$ single-crystal fibers grown by the laser-heated pedestal growth technique, Vib. Spectrosc. 73 (2014) 144–149.
[25] A. Ayala, C. Paschoal, I. Guedes, W. Paraguassu, P. Freire, J. Mendes Filho, et al., Disorder-induced symmetry lowering in the $CsInMgF_6$ pyrochlore crystal, Phys. Rev. B 66 (2002) 214105.
[26] G. Blasse, A.F. Corsmit, Vibrational spectra of 1:2 ordered perovskites, J. Solid State Chem. 10 (1974) 39–45.
[27] S. Wang, Y. Chen, S. Fang, L. Zhang, M. Tang, K. An, et al., Novel chemically stable $Ba_3Ca_{1.18}Nb_{1.82-x}Y_xO_{9-\delta}$ proton conductor: improved proton conductivity through tailored cation ordering, Chem. Mater. 26 (2014) 2021–2029.
[28] W.H. Kan, J. Lussier, M. Bieringer, V. Thangadurai, Studies on polymorphic sequence during the formation of the 1:1 ordered perovskite-type $BaCa_{(0.335)}M_{(0.165)}Nb_{(0.5)}O_{(3-\delta)}$ (M = Mn, Fe, Co) using in situ and ex situ powder X-ray diffraction, Inorg. Chem. 53 (2014) 10085–10093.
[29] M.I. Mendelson, Average grain size in polycrystalline ceramics, J. Am. Ceram. Soc. 52 (1969) 443–446.
[30] Y.W. Kim, J.H. Park, J.G. Park, Local cationic ordering behavior in $Ba(Mg_{1/3}Nb_{2/3})O_3$ ceramics, J. Eur. Ceram. Soc. 24 (2004) 1775–1779.
[31] S. Nomura, Ceramics for microwave dielectric resonator, Ferroelectrics 49 (1983) 61–70.
[32] K. Wakino, M. Murata, H. Tamura, Far infrared reflection spectra of Ba(Zn,Ta)O_3-$BaZrO_3$ Dielectric Resonator Material, J. Am. Ceram. Soc. 69 (1986) 34–37.
[33] T. Shimada, Dielectric loss and damping constants of lattice vibrations in $Ba(Mg_{1/3},Ta_{2/3})O_3$ ceramics, J. Eur. Ceram. Soc. 23 (2003) 2647–2651.
[34] M. Kuball, J.M. Hayes, Y. Shi, J.H. Edgar, Phonon lifetimes in bulk AlN and their temperature dependence, Appl. Phys. Lett. 77 (2000) 1958.
[35] L. Bergman, D. Alexson, P. Murphy, R. Nemanich, M. Dutta, M. Stroscio, et al., Raman analysis of phonon lifetimes in AlN and GaN of wurtzite structure, Phys. Rev. B 59 (1999) 12977–12982.
[36] N. Ichinose, T. Shimada, Effect of grain size and secondary phase on microwave dielectric properties of $Ba(Mg_{1/3}Ta_{2/3})O_3$ and $Ba([Mg,Zn]_{1/3}Ta_{2/3})O_3$ systems, J. Eur. Ceram. Soc. 26 (2006) 1755–1759.
[37] D.A. Sagala, S. Nambu, Microscopic calculation of dielectric loss at microwave frequencies for complex perovskite $Ba(Zn_{1/3}Ta_{2/3})O_3$, J. Am. Ceram. Soc. 75 (1992) 2573–2575.
[38] E.L. Colla, I.M. Reaney, N. Setter, Effect of structural changes in complex perovskites on the temperature coefficient of the relative permittivity, J. Appl. Phys. 74 (1993) 3414–3425.
[39] A.M. Glazer, The classification of tilted octahedra in perovskites, Acta Crystallogr. Sect. B Struct. Crystallogr. Cryst. Chem. 28 (1972) 3384–3392.
[40] I.M. Reaney, E.L. Colla, N. Setter, Dielectric and structural characteristics of Ba- and Sr-based complex perovskites as a function of tolerance factor, Jpn. J. Appl. Phys. 33 (1994) 3984–3990.
[41] C.-W. Ahn, S. Nahm, Y.-S. Lim, W. Choi, H.-M. Park, H.-J. Lee, Microstructure and microwave dielectric properties of $Ba(Co_{1/3}Nb_{2/3})O_3$ Ceramics, Jpn. J. Appl. Phys. 41 (2002) 5277–5280.
[42] K. Fukuda, R. Kitoh, I. Awai, Far-Infrared reflection spectra of dielectric ceramics for microwave applications, J. Am. Ceram. Soc. 77 (1994) 149–154.
[43] Y. Zhang, Y. Zhang, B. Fu, M. Hong, M. Xiang, Z. Liu, et al., Microstructure and microwave dielectric properties of $MgNb_2O_6$–$ZnTa_2O_6$ composite ceramics prepared by layered stacking method, J. Mater. Sci. Mater. Electron. 25 (2014) 5475–5480.